

N -photon bundles emission in high-spin Jaynes-Cummings model

Huanhuan Wei

Guangdong Provincial Key Laboratory of Quantum Metrology and Sensing & School of Physics and Astronomy, Sun Yat-Sen University (Zhuhai Campus), Zhuhai 519082, China

Jing Tang

School of Physics and Optoelectronic Engineering, Guangdong University of Technology, Guangzhou 510006, China
Guangdong Provincial Key Laboratory of Sensing Physics and System Integration Applications, Guangdong University of Technology, Guangzhou, 510006, China

Yuangan Deng

Guangdong Provincial Key Laboratory of Quantum Metrology and Sensing & School of Physics and Astronomy, Sun Yat-Sen University (Zhuhai Campus), Zhuhai 519082, China

E-mail: jingtang@gdut.edu.cn

E-mail: dengyg3@mail.sysu.edu.cn

Abstract. High-spin quantum systems, endowed with rich internal degrees of freedom, constitute a promising platform for manipulating high-quality n -photon states. In this study, we explore n -photon bundles emission by constructing a high-spin Jaynes-Cummings model (JCM) within a single-mode cavity interacting with a single spin-3/2 atom. Our analysis reveals that the n -photon dressed state splittings can be significantly enhanced by adjusting the linear Zeeman shift inherent to the internal degrees of freedom in high-spin systems, thereby yielding well-resolved n -photon resonance. The markedly enhanced energy-spectrum anharmonicity, stemming from strong nonlinearities, enables the realization of high-quality n -photon bundles emission with large steady-state photon numbers, in contrast to conventional spin-1/2 JCM setups. Of particular interest is the realization of an optical multimode transducer capable of transitioning among single-photon blockade, two- to four-photon bundles emission, and photon-induced tunneling by tuning the light-cavity detuning in the presence of both cavity and atomic pump fields. This work unveils significant opportunities for diverse applications in nonclassical all-optical switching and high-quality multiphoton sources, deepening our understanding of creating specialized nonclassical states and fundamental physics in high-spin atom-cavity systems.

Keywords: Spin-3/2 JCM, Photon blockade, N -photon bundles, Optical multimode transducer

1. Introduction

Multiphoton states, serving as fundamental elements of quantum lights, provide versatile applications in quantum communication [1], quantum computing [2, 3], quantum metrology [4, 5] and fundamental examinations of quantum physics [6, 7]. A pivotal means to generate these states is through n -photon blockade (PB) [8], which is known as nonlinear quantum scissors [9]. This effect transforms classical light into non-classical light, by impeding the generation of the subsequent photons when n photons are present, drawing substantial attention due to its potential applications in quantum information and communication.

Creating single-PB relies on two typical physical mechanisms. One is the conventional PB, with requiring a sufficiently large energy-spectrum anharmonicity [10, 11]. The other is unconventional PB, operating via destructive quantum interference among various quantum transition pathways [12, 13, 14]. Both these PB types have been extensively investigated across various quantum systems, encompassing cavity quantum electrodynamics (QEDs) systems [15, 16, 17, 18, 19], superconducting circuit QED systems [20, 21], Kerr-type nonlinear cavities [22, 23, 24, 25], and optomechanical systems [26, 27, 28, 29]. At the same time, 2-PB has been theoretically proposed and experimentally advanced in Kerr-type system [30, 31], strong-coupling qubit-cavity system [32, 33], and a cascaded cavity QED system [31, 34]. Furthermore, investigations into n -PB ($n > 2$) have also been explored [35, 36, 37, 38]. The mechanism for generating n -PB relies on the great strong energy-spectrum anharmonicity. Notably, achieving n -PB through the unconventional mechanism, involving intricate conditions of destructive quantum interference, poses significant challenges.

In contrast to the extensively studied n -PB, the emission of n -photon bundles, representing a new building block in quantum optics, releases bundles of strongly correlated photons, offering opportunities for exploring fundamental physics and applications in quantum information science and technology [39, 40, 41, 42]. The n -photon bundles states exhibit strong bunching for single photons and antibunching for separate bundles of photons. Mechanisms for generating n -photon (phonon) bundles include n -phonon resonance processes [43], Mollow physics [44, 45, 46, 47], deterministic parametric down-conversion [48, 49, 50], Stokes multiphonon processes [51] and parity-symmetry-protected multiphoton processes [52]. These significant advances have predominantly focused on generating high-purity n -quanta states utilizing the standard two-level Jaynes-Cummings model (JCM) under strong coupling conditions, posing experimental challenges in cavity QEDs. Recently, high-quality non-classical single-photon to two-photon bundles emission has been proposed in a spin-1 JCM [53]. This proposal benefits from the large internal degrees of freedom, overcoming experimental constraints associated with strong atom-cavity coupling. Leveraging the internal degrees of freedom in high-spin systems, this mechanism opens new avenues for creating exotic nonclassical states and offers versatile applications in quantum information and metrology.

In this work, we propose to the generation of n -photon bundles emission utilizing a single atom trapped in a single-mode optical cavity with constructing a spin-3/2 JCM. We demonstrate the n -photon resonance can be finely tuned by manipulating the linear Zeeman shift, facilitated by the internal degrees of freedom inherent in the high-spin atom-cavity system. By independently driving the cavity field and atom pump field, high-quality single-PB and two-photon bundles emission are observed, respectively. We show that the generalized second-order correlation functions for single-photon and two-photon bundles states can reach values as low as $g_1^{(2)}(0) \approx 7.3 \times 10^{-4}$ and $g_2^{(2)}(0) \approx 6.6 \times 10^{-4}$, respectively. These results indicate strong sub-Poissonian photon statistics for single photons and isolated two-photon bundles. Remarkably, we demonstrate the feasibility of an optical multimode transducer capable of transitioning among various photon states: ranging from single-PB to multiphoton bundles, as well as photon-induced tunneling (PIT). This broadens the horizon for diverse technological applications, spanning from nonclassical multimode transducers to high-quality multiphoton sources [54, 55, 56].

In contrast to the quadratic Zeeman shift utilized in spin-1 JCM [53], the novelty lies in the distinct physical mechanism governing the generation of strong energy-spectrum anharmonicity leveraging the linear Zeeman shift. Thus we achieve three-photon and four-photon bundles emission with large steady-state photon numbers under simultaneous action of cavity-driven and atom-pump fields. These high-quality n -photon bundles state showcasing distinct statistical properties of photon bunching for single photons with $g_1^{(2)}(0) > g_1^{(2)}(\tau)$ and antibunching for separated ones with $g_n^{(2)}(0) < g_n^{(2)}(\tau)$, play a pivotal role in quantum metrology [4, 5], quantum lithography and cryptography [40, 57]. Compared to creating n -photon bundle states typically relying on Mollow physics [44, 45, 46, 47], which depend on high-order processes operated in the far dispersive regime, our proposal benefits from the large internal degrees of freedom inherent to introduce a novel mechanism for significantly enhancing energy-spectrum anharmonicity in high-spin systems.

The paper is structured as follows: In Sec. 2, we introduce the model and Hamiltonian responsible for realizing n -photon bundles emission in the spin-3/2 JCM system. In Sec. 3, we calculate the energy spectrum of the system. Sec. 4 outlines the conditions necessary for achieving n -photon bundles emission. Sec. 5 showcases the outcomes of numerical simulations concerning n -photon bundles emission. Finally, Sec. 6 offers a concise summary of our results.

2. Model and Hamiltonian

To generate n -photon bundles emission, we consider a high-finesse single alkaline-earth-metal (like) atom confined in a single-mode optical cavity, driven by a weak laser field with amplitude η and frequency ω_L , as depicted in Fig. 1(a). The atomic energy-level structure for the pseudo-spin 3/2 atom is illustrated in Fig. 1(b). This structure our internal magnetic Zeeman levels of the ground states $|b_j\rangle$ with $j = 1, 2, 3, 4$ and three

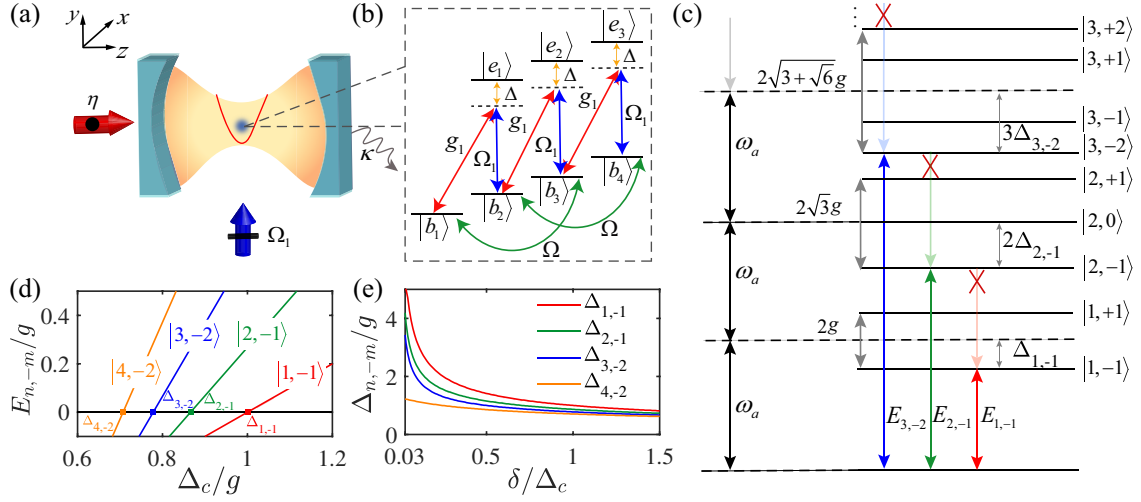


Figure 1. (color online). (a) Sketch of a single atom inside a high-finesse optical cavity for generating n -photon bundles emission. (b) Level diagram for a single spin-3/2 atom. (c) Anharmonicity energy spectrum of Hamiltonian (2) for $\delta = \Delta_c$. The energy splitting of the n th dressed states $|n, \pm m\rangle$ is determined using the analytic expression in Eq. (4). (d) Δ_c dependence of energy spectrum $E_{n,-m}$ with square denoting the positions of n -photon resonance $\Delta_{n,-m}$ ($m = 1, 2$). (e) Variation of n -photon resonance $\Delta_{n,-m}$ ($m = 1, 2$) as a function of δ .

electronically excited states $|e_j\rangle$ with $j = 1, 2, 3$. A bias magnetic field \mathbf{B} along the cavity axis is defined as the quantization axis (z -axis), induces a significant Zeeman shift $\hbar\omega_b$ within the ground state manifold.

Regarding the optical cavity, its bare frequency and decay rate are denoted as ω_c and κ , respectively. In our scheme, a σ^+ -polarized cavity field is far-off resonant with the atomic transitions $|b_j\rangle \leftrightarrow |e_j\rangle$, corresponding to the single-atom cavity coupling strength g_1 and atom-cavity detuning Δ . To generate the Raman coupling, the atomic transitions $|b_{j+1}\rangle \leftrightarrow |e_j\rangle$ are coupled by a π -polarized classical pump field perpendicular to the cavity axis with Rabi frequency Ω_1 . The magnetic quantum numbers of the electronic states satisfy $m_{|b_j\rangle} = m_{|e_j\rangle} - 1$ and $m_{|b_{j+1}\rangle} = m_{|e_j\rangle}$. Additionally, we consider the next nearest neighbors of ground states through a pair of σ -polarized classical laser fields, inducing the atomic transitions $|b_j\rangle \leftrightarrow |b_{j+2}\rangle$ with a weak Rabi frequency of Ω , as illustrated in Fig. 1(b). The frequency difference between the pair laser is adjusted to compensate for the Zeeman shift between $|b_j\rangle$ and $|b_{j+2}\rangle$ states. It is important to note that, in this laser configuration, the laser frequency responsible for the effective atomic pumping is significantly detuned from the cavity resonance frequency.

In the case of large atom-cavity detuning limit, $g_1/\Delta \ll 1$ and $\Omega_1/\Delta \ll 1$, the three far-off resonance excited states $|e_j\rangle$ with $j = 1, 2, 3$ can be adiabatically eliminated. Using the rotating-wave approximation, we can formulate the Hamiltonian describing the spin-3/2 JCM system along with the driving terms corresponding to the cavity field

and the atomic pump field (refer to Appendix A).

$$\begin{aligned} \hat{H}_1/\hbar = & \Delta_c \hat{a}^\dagger \hat{a} + \Delta_a \sum_{j=1}^3 j \hat{b}_{j+1}^\dagger \hat{b}_{j+1} + \eta(\hat{a}^\dagger + \hat{a}), \\ & + \left[g \hat{a}^\dagger \sum_{j=1}^3 \hat{b}_j^\dagger \hat{b}_{j+1} + \Omega \sum_{j=1}^2 \hat{b}_j^\dagger \hat{b}_{j+2} + \text{H.c.} \right], \end{aligned} \quad (1)$$

where $\hat{a}^\dagger(\hat{a})$ is the creation (annihilation) operator for the cavity mode and \hat{b}_j^\dagger (\hat{b}_j) represents the atomic spin projection operator for the four relevant states with $j = 1, 2, 3, 4$. $\Delta_c = \Delta'_c - g_1^2/\Delta$ is the effective cavity-light detuning, $\Delta_a = \omega_b - |\Omega_1|^2/\Delta$ is the tunable effective single photon detuning of atom, and $g = -g_1\Omega_1/\Delta$ is the effective atom-cavity coupling.

To gain more insight of photon emissions, the spin-3/2 representation of the Hamiltonian (1) with neglecting the weak driving fields can be reformulated as:

$$\hat{H}_2/\hbar = \Delta_c \hat{a}^\dagger \hat{a} + \delta \hat{S}_z + g(\hat{a} \hat{F}_+ + \hat{a}^\dagger \hat{F}_-). \quad (2)$$

Here $\delta = \Delta_a$ is the effective linear Zeeman shift and \hat{S}_z denotes the spin-3/2 matrices with the angular momentum operator defined as $\hat{S}_z = \sum_{j=1}^4 (j - \frac{5}{2}) \hat{b}_j^\dagger \hat{b}_j$. For convenience of representation, the atomic transition matrix is denoted by \hat{F}_+ (\hat{F}_-), where the raising operator is expressed as $\hat{F}_+ = \sum_{j=1}^3 \hat{b}_{j+1}^\dagger \hat{b}_j$ with $\hat{F}_+ = \hat{F}_-^\dagger$.

3. Energy spectrum of the system

To explore the physical processes of multiphoton bundles emission, the energy spectrum of the system is calculated by diagonalizing Hamiltonian in Eq. (2). The total number of excitations operator $\hat{N} = \hat{a}^\dagger \hat{a} + \hat{S}_z + 3/2$ is conserved within our system and satisfies the commutation relation $[\hat{N}, \hat{H}_2] = 0$ when dissipative and driving fields for the atom and cavity are neglected. By fixing the total excitation number, the relevant Hilbert space of atom-cavity system is restricted to the states $|n, b_1\rangle, |n-1, b_2\rangle, |n-2, b_3\rangle, |n-3, b_4\rangle$, where n denotes the number of photon excitations. The corresponding matrix is obtained by solving the Schrödinger equation $\hat{\mathcal{H}}\Psi = M\Psi$, utilizing the associated basis states $\Psi = [|n, b_1\rangle, |n-1, b_2\rangle, |n-2, b_3\rangle, |n-3, b_4\rangle]^T$. Consequently, the matrix M is explicitly represented as

$$M = \begin{pmatrix} n\Delta_c & \sqrt{n}g & 0 & 0 \\ \sqrt{n}g & (n-1)\Delta_c + \delta & \sqrt{n-1}g & 0 \\ 0 & \sqrt{n-1}g & (n-2)\Delta_c + 2\delta & \sqrt{n-2}g \\ 0 & 0 & \sqrt{n-2}g & (n-3)\Delta_c + 3\delta \end{pmatrix}. \quad (3)$$

After the diagonalization matrix (3), the energy spectrum of n th ($n \geq 3$) dressed state in the spin-3/2 JCM is reclassified into four distinct branches. Specifically, the

first dressed state splits into two branches ($|1, +1\rangle$ and $|1, -1\rangle$), while the second dressed state divides into three branches ($|2, +1\rangle, |2, 0\rangle$, and $|2, -1\rangle$), as indicated in Fig. 1(c).

Explicitly, the energy eigenvalues for n -photon excitations ($n \geq 3$) for the fixed $\delta/\Delta_c = 1$ are given by

$$\begin{aligned} E_{n,\pm 1} &= n(\Delta_c - \Delta_{n,\pm 1}), \\ E_{n,\pm 2} &= n(\Delta_c - \Delta_{n,\pm 2}), \end{aligned} \quad (4)$$

corresponding the n -photon resonance ($\Delta_{n,\pm m}$) of the involved dressed states $|n, \pm m\rangle (m = 1, 2)$ satisfying

$$\begin{aligned} \Delta_{n,\pm 1} &= \mp \sqrt{\frac{3n - 3 - \sqrt{5n^2 - 10n + 9}}{2n^2}}g, \\ \Delta_{n,\pm 2} &= \mp \sqrt{\frac{3n - 3 + \sqrt{5n^2 - 10n + 9}}{2n^2}}g. \end{aligned}$$

here $|n, \pm 2\rangle$ index the highest and lowest branches of the splitting states, while $|n, \pm 1\rangle$ index the higher and lower two branches. The energies $E_{n,\pm m} (m = 1, 2)$ correspond to the states $|n, \pm m\rangle$. In Fig. 1(c), we present the typical anharmonicity ladder of the energy spectrum for spin-3/2 JCM. Notably, the asymmetric energy splittings of the n th dressed states ($n > 2$) for the lower $|n, m = -1\rangle$ and lowest $|n, m = -2\rangle$ branches are labeled as $n\Delta_{n,-1}$ and $n\Delta_{n,-2}$, respectively.

Figure 1(e) characterizes the n -photon resonance $\Delta_{n,-m} (m = 1, 2)$ as a function of δ . As can be seen, the n -photon resonance gradually decreases as δ increases until it converges at $\delta/\Delta_c = 1$ with the fixed number of cavity excitations. Additionally, when fixing δ/Δ_c , the value of single-photon resonance is bigger than the two-photon resonance, and the two-photon resonance outweighs the three-photon resonance ($\Delta_{1,-1} > \Delta_{2,-1} > \Delta_{3,-2}$), which agrees well with the values in Fig. 1(d). We should note that a smaller detuning ratio δ/Δ_c results in a considerably larger n -photon dressed state splitting. Explicitly, the n th dressed state splitting exhibits a symmetrical structure manifesting n -photon resonance, satisfying $\Delta_{n,+2} = -\Delta_{n,-2}$.

4. Simulation method

To investigate the relevant quantum properties of the spin-3/2 JCM system, including the drive and dissipation of the cavity field and the atom pump field [31], we calculate the steady state solution by numerically solving the quantum master equation using the Quantum Optics Toolbox [58]. Specifically, the time evolution of the density matrix ρ is governed by the master equation, $d\rho/dt = \mathcal{L}\rho$. The Liouvillian superoperator \mathcal{L} associated with the Lindblad-type master equation is defined as

$$\mathcal{L}\rho = -i[\hat{H}_1, \rho] + \frac{\kappa}{2}\mathcal{D}[\hat{a}]\rho + \frac{\gamma}{2}\mathcal{D}[\hat{F}_-]\rho, \quad (5)$$

where ρ is density matrix of the atom-cavity system, γ is the spontaneous emission rate of the atom, and $\mathcal{D}[\hat{o}]\rho = 2\hat{o}\rho\hat{o}^\dagger - \hat{o}^\dagger\hat{o}\rho - \rho\hat{o}^\dagger\hat{o}$ represents the Lindblad type of dissipation.

It's worth noting that, for the ground state of atom, the effect of weak pure dephasing can be disregarded.

For the k -th order correlation function related to a time interval τ for n -photons, a significant physical quantity in quantum statistics, is described by [45, 43]:

$$g_n^{(k)}(\tau_1, \dots, \tau_n) = \frac{\langle \prod_{i=1}^k [\hat{a}^\dagger(\tau_i)]^n \prod_{i=1}^k [\hat{a}(\tau_i)]^n \rangle}{\prod_{i=1}^k \langle [\hat{a}^\dagger(\tau_i)]^n [\hat{a}(\tau_i)]^n \rangle} \quad (6)$$

In the realm of individual photons, the general k -order correlation function is represented as $g_1^{(k)}(\tau)$. Conversely, the quantum characteristic of emitted multiphoton bundles emission are captured by the correlation function for n -photons, denoted as $g_n^{(k)}(\tau_1, \dots, \tau_n)$ [59]. Additionally, the derivation of the multiphoton correlation function can be involved the application of the quantum regression theorem [60].

The quantum properties of n -PB are fundamentally characterized by the correlation functions, which are derived from the steady-state density matrix obtained by numerically solving $\mathcal{L}\rho_s = 0$. Subsequently, the corresponding number of steady-state photons, denoted as $n_s = \text{Tr}(\hat{a}^\dagger \hat{\rho}_s)$, can be calculated. The correlation function for n -PB [31, 38] is expected to satisfy the following criteria:

$$g_1^{(n)}(0) > 1 \text{ and } g_1^{(n+1)}(0) < 1. \quad (7)$$

These conditions reveal the simultaneous presence of n th-order super-Poissonian photon statistics and $(n + 1)$ th-order sub-Poissonian photon statistics. This implies that the excitation of the first n photons will block the transmission of the subsequent $(n + 1)$ th photon, leading to an orderly output of n -photon stream with sub-Poissonian statistics.

For n -photon bundles state ($n > 1$), two additional conditions, $g_1^{(2)}(0) > g_1^{(2)}(\tau)$ and $g_n^{(2)}(0) < g_n^{(2)}(\tau)$, are required to guarantee photon bunching for the isolated photons and photon anti-bunching for the detached n -photon bundles [43, 45, 48]. Specifically, single-PB is characterized by criteria $g_1^{(2)}(0) < 1$ and $g_1^{(2)}(0) < g_1^{(2)}(\tau)$, to guarantee the sub-Poissonian photon statistics and photon antibunching. A low value of $g_1^{(2)}(0)$ indicates a higher purity of single-photon emission. It is noted that $g_1^{(2)}(0) = 0$ corresponds to an ideal single photon blockade with complete suppression of multiphoton excitations. Conversely, the criterion $g_1^{(n)}(0) > 1$ (for $n = 2, 3, 4, 5$) is utilized to identify the PIT effect [38], demonstrating super-Poissonian photon statistics [61].

5. Numerical results

In this section, we present the results of numerical simulations, illustrating the feasibility of achieving n -photon bundles emission in a spin-3/2 JCM featuring an effective $F = 3/2$ alkaline-earth metal atom [62, 63, 64]), confined in a high-precision cavity in the current experimental setup. Conventionally, we designate the decay rate of the optical cavity as $\kappa = 2\pi \times 160$ kHz, serving as the representative energy unit of the system [64]. Consequently, the long-lived decay rate of the atomic ground state can be safely neglected due to experimentally feasible assumption. The coupling strength of the

single atomic cavity is considered to be $g/\kappa = 20$. Without loss of generality, we adopt $g_1^{(2)}(0) < 0.01$ and $g_n^{(2)}(0) < 0.01$ as benchmarks for high-quality single-PB and n -photon bundle emission. In addition to strong sub-Poissonian statistics with $g_n^{(2)}(0) \ll 1$, the photon antibunching is further verified by $g_n^{(2)}(0) < g_n^{(2)}(\tau)$ using the quantum regression theorem. The tunable parameters in our system encompass the light-cavity detuning Δ_c , cavity driven strength η , Rabi frequency of the classical pump field Ω , and linear Zeeman shift δ .

5.1. Strong single-PB

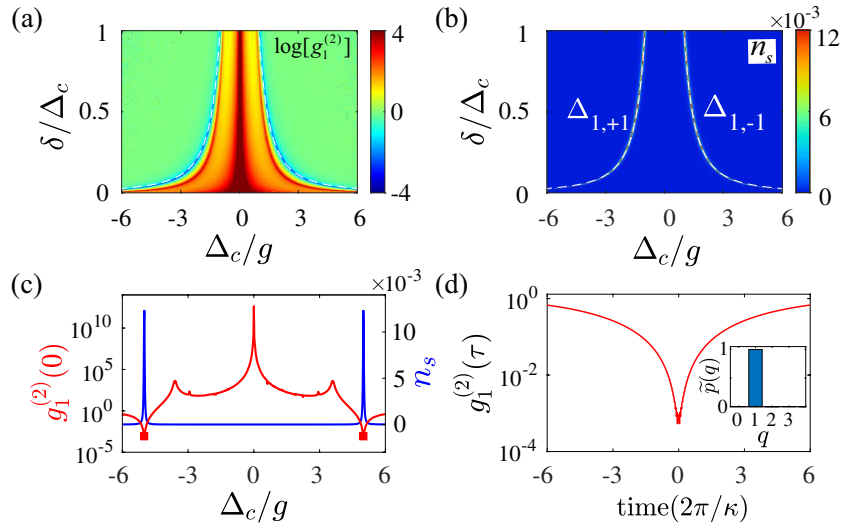


Figure 2. (color online) Statistical characteristics of photons in a spin-3/2 JCM with cavity driving. Distributions of (a) equal time second-order correlation function $g_1^{(2)}(0)$ and (b) the corresponding n_s on the Δ_c - δ parameter plane. (c) $g_1^{(2)}(0)$ (red line) and n_s (blue line) as a function of Δ_c for $\delta/\Delta_c = 0.04$. (d) Time interval τ dependence of $g_1^{(2)}(\tau)$ for $\delta/\Delta_c = 0.04$ and $\Delta_c/g = \pm 5$. The inset in (d) depicts the steady-state photon-number distribution $\tilde{p}(q)$ at the single-photon resonances. The other parameters are $\eta/\kappa = 0.1$ and $\Omega/\kappa = 0$.

To attain strong single-PB, we initially consider the weak cavity field regime with $\eta/\kappa = 0.1$ in the spin-3/2 JCM system, while maintaining the pumping field at $\Omega/\kappa = 0$. We have checked that the energy spectrum remains almost unchanged due to the sufficiently weak cavity-driven amplitudes ($\eta/g \ll 1$ and $\Omega/g \ll 1$). Indeed, n -photon resonance is slightly shift even for $\eta/g \sim 1$ and $\Omega/g \sim 1$ [65]. Figures 2(a) and 2(b) illustrate the logarithmic plot of the equal-time second-order correlation function $g_1^{(2)}(0)$ and the corresponding steady-state cavity photon number n_s as functions of the light cavity detuning Δ_c and the linear Zeeman shift δ . It is evident that both $g_1^{(2)}(0)$ and n_s exhibit a red-blue symmetric profile with respect to the light-cavity detuning $\Delta_{1,-1} = -\Delta_{1,+1}$ (dashed white lines). Notably, strong single-PB with $g_1^{(2)}(0) < 0.01$ is realized at the vacuum Rabi splitting $\Delta_{1,\pm 1}$, accompanied by significant steady-state intracavity photon emission.

For a more clearer illustration of the strong single-PB, Figure 2(c) displays $g_1^{(2)}(0)$ and n_s versus Δ_c/g with fixing $\delta/\Delta_c = 0.04$. The photon quantum statistics demonstrate a strong PB with $g_1^{(2)}(0) \approx 7.3 \times 10^{-4}$ at the red and blue sidebands of the single-photon resonance $\Delta_{1,\pm 1}/g = \mp 5$, corresponding to a larger cavity photon number with $n_s \approx 0.012$. Particularly, the single-photon resonance points $\Delta_{1,\pm 1}/g = \mp 5$ agree well with the analytically derived energy spectrum as displayed in Fig. B1(a) (see Appendix B). Figure 2(d) shows the time evolution of the second-order correlation function $g_1^{(2)}(\tau)$ at $\delta/\Delta_c = 0.04$ and the single-photon resonance with $\Delta_{1,-1}/g = 5$. Evidently, photon antibunching characterized by $g_1^{(2)}(0) < g_1^{(2)}(\tau)$ is observable. It's crucial to emphasize that the lifetime of single photon antibunching is dominated by the cavity decay rate, which is proportional to $1/\kappa = 6.25$ ms.

To provide further verification of the single-PB characteristic, photon-number distribution is depicted by the ratio of q -photon state to the total number of excited photons, i.e., $\tilde{p}(q) = qp(q)/n_s$, where $p(q) = \text{Tr}(|q\rangle\langle q|\rho_s)$ refers to the steady-state photon number distribution (inset of Fig. 2(d)). This representation indicates that the photon emission for predominantly comprises single photons, reaching nearly 100% at $\Delta_c/g = \Delta_{1,\pm 1}$. The observed strong single-PB can be attributed to the anharmonicity of the energy spectrum induced by tuning the linear Zeeman shift δ , as illustrated in the ladder diagram of Fig. 1(c) for the spin-3/2 JCM system. For instance, when the laser field is tuned to resonance with the first excited state ($|1, -\rangle$) at $\delta/\Delta_c=1$, the system's second energy eigenstate ($|2, -\rangle$) becomes off-resonant, exhibiting an energy gap of $(2 - \sqrt{3}/2)g$. This configuration significantly suppresses two-photon excitations, leading to the pronounced manifestation of single-PB effect.

5.2. High-quality two-photon bundles emission

In this section, we focus on the quantum characteristics of two-photon bundles emission under the influence of a weak pumping field, with Ω/κ held constant at 0.05 ($\eta/\kappa = 0$). Figures 3(a)-(c) display the correlation functions $g_1^{(2)}(0)$ and $g_1^{(3)}(0)$ on a logarithmic scale, as well as the steady-state cavity photon number n_s , as functions of the detuning Δ_c and the linear Zeeman shift δ . Notably, at the two-photon resonance points $\Delta_{2,\pm 1}$, as indicated by dashed lines, we observe a super-Poissonian distribution ($g_1^{(2)}(0) > 1$) and a sub-Poissonian distribution ($g_1^{(3)}(0) < 1$) for the emitted photons, accompanied by significant photon emission. This observation signifies the formation of 2-PB. Interestingly, the central branch at $\Delta_c = 0$ also exhibits substantial photon emission, characterized by $g_1^{(2)}(0) > 1$ and $g_1^{(3)}(0) < 1$, confirming the generation of the 2-PB effect.

Figures 3(d) and 3(e) depict $g_1^{(n)}(0)$ (for $n = 2, 3$) and n_s as a function of Δ_c , with $\delta/\Delta_c = 0.07$. These figures reveal the implementation of strong 2-PB, with $g_1^{(2)}(0) \approx 1.45$ and $g_1^{(3)}(0) \approx 6.6 \times 10^{-4}$ at the two-photon resonance points $\Delta_{2,\pm 1}/g = \mp 2.7$. Simultaneously, the maximum photon emission n_s is observed at the two-photon resonances, serving as another crucial indicator of a high-quality two-

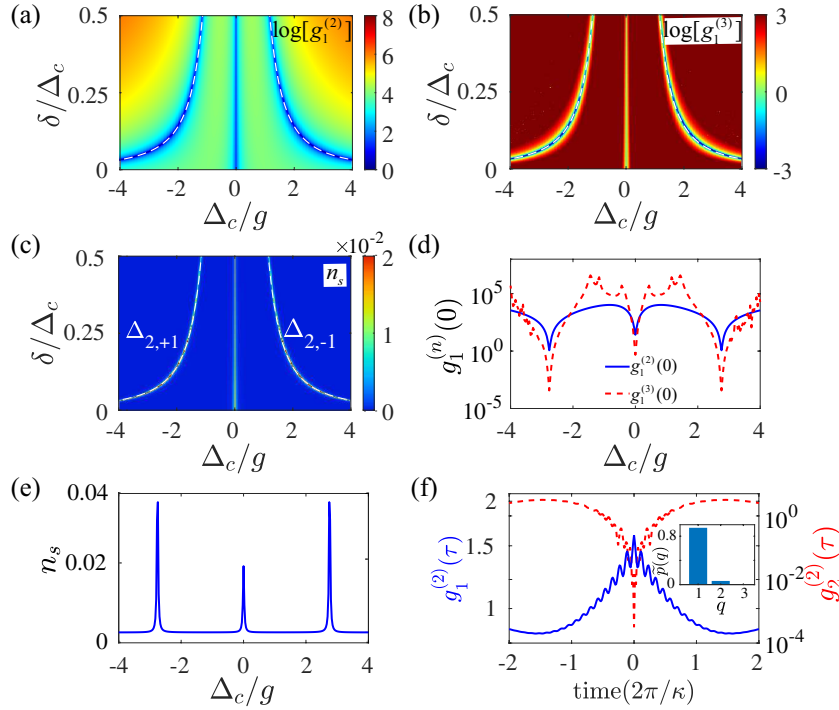


Figure 3. (Color online) The statistical properties of photons in a spin-3/2 JCM with atom pump field. Contour plots of (a) $\log[g_1^{(2)}(0)]$, (b) $\log[g_1^{(3)}(0)]$ and (c) n_s as functions of Δ_c and δ . The Δ_c dependence of (d) $g_1^{(2)}(0)$ (blue solid line) and $g_1^{(3)}(0)$ (red dashed line), and (e) n_s with $\delta/\Delta_c = 0.07$. (f) Time interval τ dependence of $g_1^{(2)}(\tau)$ (blue solid line) and $g_2^{(2)}(\tau)$ (red dashed line) for $\delta/\Delta_c = 0.07$ and $\Delta_c/g = \pm 2.7$. The white dashed lines in (a)-(c) show the analytical two-photon resonance $\Delta_{2,\pm 1}$ of the second dressed state in the energy spectrum. Additionally, the inset in (f) plots $\tilde{p}(q)$ at two-photon resonances $\Delta_c/g = \pm 2.7$. The other parameters are $\Omega/\kappa = 0.05$ and $\eta/\kappa = 0$.

photon source. Remarkably, the photon emission of the central branch at $\Delta_c = 0$ also aligns with the 2-PB characteristics, exhibiting super-Poissonian statistics ($g_1^{(2)}(0) > 1$) and sub-Poissonian statistics ($g_1^{(3)}(0) < 1$) for photon distribution. As shown in the inset of Fig. 3(f), the two-photon emission nature is evidenced by the photon number distribution $\tilde{p}(q)$, which becomes negligible when $q > 2$. The underlying mechanism for generating the strong 2-PB effect mirrors that of single photons, both attributed to the anharmonicity of the energy spectrum by tuning the linear Zeeman shift in the spin-3/2 JCM system. The off-resonant energy gap between the second and fourth energy eigenstates at $\delta/\Delta_c=1$ are $2(\sqrt{3} - \sqrt{2})g$, which suppresses four-photon excitations, leading to the strong 2-PB effect.

To further elucidate the nature of two-photon bundles emission, Figure 3(f) shows $g_1^{(2)}(\tau)$ and $g_2^{(2)}(\tau)$ plotted against the time interval τ at the two-photon resonance $\Delta_{2,\pm 1}/g = \mp 2.7$. It is evident that $g_1^{(2)}(0) > g_1^{(2)}(\tau)$ and $g_2^{(2)}(0) < g_2^{(2)}(\tau)$, confirming the occurrence of single-photon bunching and two-photon bundles anti-bunching. This result signifies the successful emission of two-photon bundles. Additionally, the decay

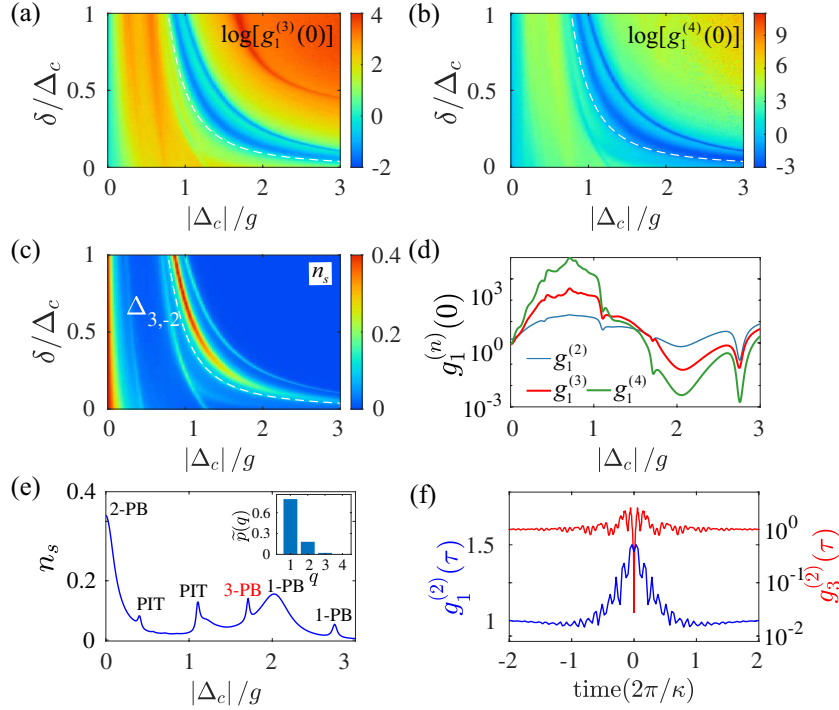


Figure 4. (Color online) The statistical characteristics of photons in a spin-3/2 JCM with cavity and atom pump field. Distributions of (a) $g_1^{(3)}(0)$, (b) $g_1^{(4)}(0)$ and (c) n_s on the $|\Delta_c|$ - δ parameter plane. (d) $g_1^{(2)}(0)$ (blue line), $g_1^{(3)}(0)$ (red line), $g_1^{(4)}(0)$ (green line), and (e) the corresponding n_s as a function of $|\Delta_c|$ for $\delta/\Delta_c = 0.13$. (f) Time interval τ dependence of $g_1^{(2)}(\tau)$ (blue line) and $g_3^{(2)}(\tau)$ (red line) for $\delta/\Delta_c = 0.13$ and $\Delta_c/g = \pm 1.7$. The white dashed lines in (a), (b) and (c) show the analytical three-photon resonance $\Delta_{3,\pm 2}$ of the third dressed state of the energy spectrum. The inset in (e) plots $\tilde{p}(q)$ at the three-photon resonances $\Delta_c/g = \pm 1.7$. The other parameters are $\eta/\kappa = 0.3$ and $\Omega/\kappa = 1.3$.

timescales of single-photon bunching and separated two-photon anti-bunching are comparable, both being proportional to $1/\kappa$.

5.3. Three-photon bundles emission

To explore the statistical properties of three-photon bundles emission, we consider both a large cavity drive with $\eta/\kappa = 0.3$ and a Rabi frequency of the pump field with $\Omega = 1.3$. Notably, Figs. 4(a)-4(e) present the quantum statistical properties concerning the red detuning, as both $g_1^{(n)}(0)$ and n_s exhibit red-blue symmetric structures with the optical cavity detuning. Figures 4(a)-4(c) present the quantum statistics of $\log[g_1^{(3)}(0)]$, $\log[g_1^{(4)}(0)]$ and n_s , respectively, across the $|\Delta_c|$ - δ parameter plane. It is observed that at the three-photon resonance $\Delta_{3,-2}/g$ (white dashed line), a three-photon super-Poissonian distribution and a four-photon sub-Poissonian distribution are indicated by $g_1^{(3)}(0) > 1$ and $g_1^{(4)}(0) < 1$, alongside the corresponding steady-state photon numbers, demonstrating the creation of 3-PB.

Figures 4(d) and 4(e) demonstrate the values of $g_1^{(n)}(0)$ ($n = 2, 3, 4$) and n_s as a

function of $|\Delta_c|$ for $\delta/\Delta_c = 0.13$. At the three-photon resonance point $\Delta_{3,-2}/g = 1.7$, we find $g_1^{(3)}(0) = 1.35$ and $g_1^{(4)}(0) = 0.03$, indicating the generation of 3-PB. Furthermore, significant steady-state photon numbers n_s are observed, highlighting the potential for applications in three-photon sources. The three-photon nature is also illustrated by the photon-number distributions $\tilde{p}(q)$, as shown in the inset of Figure 4(e), exhibiting strong fraction of photon emission from the single-, two-, and three-photon states, while negligible photon emission occurs for $q > 3$. Additionally, at the single-photon resonance point $\Delta_{1,-1}/g = 2.7$, and the two-photon resonance point $\Delta_{2,-1}/g = 2.04$, single-PB effect are observed, with sub-Poissonian photon statistics $g_1^{(2)}(0) < 1$. Meanwhile, 2-PB effect is achieved at the two-photon resonance $\Delta_{2,0}/g = 0$, realizing 2-PB with $g_1^{(2)}(0) = 1.4$ and $g_1^{(3)}(0) = 0.8$. Interestingly, at the four-photon resonance $\Delta_{4,-2}/g = 1.1$, PIT effect is implemented as a manifestation of $g_1^{(4)}(0) > g_1^{(3)}(0) > g_1^{(2)}(0) > 1$. These pieces of evidence suggest that a quantum transducer between the single-, 2-, 3-PB and PIT effect is achieved. Notably, these resonance points correspond well with specific features in the energy spectrum, as shown in Fig. B1(c) (see Appendix B).

To further substantiate the characteristics of three-photon bundles emission, Fig. 4(f) displays $g_1^{(2)}(\tau)$ and $g_3^{(2)}(\tau)$ at the three-photon resonances $\Delta_{3,\pm 2}/g = \mp 1.7$. Evidently, single-photon bunching ($g_1^{(2)}(0) > g_1^{(2)}(\tau)$) and antibunching for isolated three-photon bundles ($g_3^{(2)}(0) < g_3^{(2)}(\tau)$) are confirmed, indicative of three-photon bundles emission. Importantly, the lifetime of the bunching associated with single photons and the antibunching related to the isolated three-photon bundles share the same timescale.

5.4. Transducer of three-photon to four-photon bundles emission

To probe the multiphoton blockade, we integrate a cavity drive with amplitude $\eta/\kappa = 0.3$ and an atomic pump field with Rabi frequency $\Omega/\kappa = 2.3$. For enhanced clarity, we emphasize the statistical properties of photons, concerning red detuning, given the red-blue symmetric nature of both $g_1^{(n)}(0)$ and n_s relative to the cavity detuning. Figures 5(a)-(c) depict numerical findings for $g_1^{(4)}(0)$, $g_1^{(5)}(0)$, and n_s as functions of $|\Delta_c|$ and δ . Notably, we discern super-Poissonian statistics for four-photons ($g_1^{(4)}(0) > 1$) and sub-Poissonian statistics for five-photons ($g_1^{(5)}(0) < 1$) at the four-photon resonance $\Delta_{4,-2}$ (indicated by red dashed line), indicating successful generation of 4-PB. The corresponding region also shows a significant photon number, as illustrated in Fig. 5(c).

To enhance our understanding of 4-PB generation, we depict n_s and $g_1^{(n)}(0)$ ($n = 2, 3, 4, 5$) as functions of $|\Delta_c|$, with $\delta/\Delta_c = 0.54$, as shown in Figs. 5(d) and 5(e). At the four-photon resonance with $\Delta_{4,-2}/g = 0.84$, we confirm the generation of 4-PB, evidenced by $g_1^{(4)}(0) = 1.49$ and $g_1^{(5)}(0) = 0.3$. The four-photon emission characteristics are further validated by the photon-number distribution $\tilde{p}(q)$, wherein negligible small values for $q > 4$, possessing the similar statistical properties observed in three-photon emission, as shown in the inset of Fig. 5(f). Simultaneously, 3-PB is achieved at the three-photon resonance with $\Delta_{3,-2}/g = 0.98$, displaying three-photon

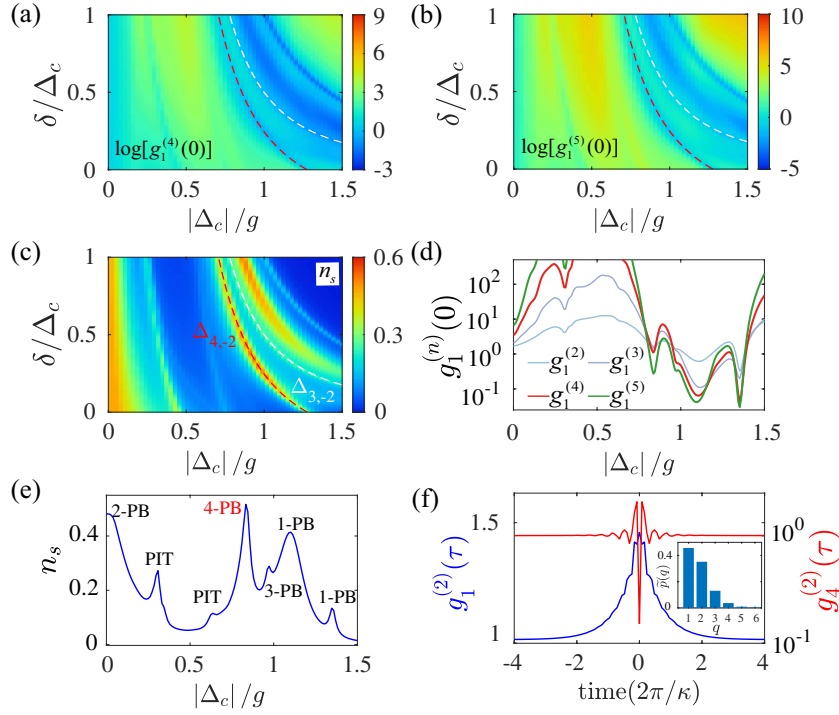


Figure 5. (Color online) Investigation of the transduction process from three-photon to four-photon bundles emission in a spin-3/2 JCM. Logarithmic plots depicting (a) $g_1^{(4)}(0)$, (b) $g_1^{(5)}(0)$ and (c) n_s as functions of $|\Delta_c|$ and δ . (d) and (e) showcase the correlation function $g_1^{(2)}(0)$, $g_1^{(3)}(0)$, $g_1^{(4)}(0)$ (red line), and $g_1^{(5)}(0)$ (green line), alongside the corresponding photon number n_s as a function of $|\Delta_c|$ with $\delta/\Delta_c = 0.54$. (f) Time interval τ dependence of $g_1^{(2)}(\tau)$ (blue line) and $g_4^{(2)}(\tau)$ (red line) for $\delta/\Delta_c = 0.54$ and $\Delta_c/g = \pm 0.84$. Insets in (f) plots the steady-state photon-number distribution $\tilde{p}(q)$ at the four photon resonances $\Delta_{c}/g = \pm 0.84$. The white and red lines in (a), (b), and (c) represent the three-photon ($\Delta_{3,-2}$) and four-photon resonances ($\Delta_{4,-2}$) for the third and fourth dressed states of the energy spectrum, respectively. The other parameters are $\Omega/\kappa = 2.3$ and $\eta/\kappa = 0.3$.

super-Poissonian statistics with $g_1^{(3)}(0) = 1.5$ and four-photon sub-Poissonian statistics with $g_1^{(4)}(0) = 0.5$. Intriguingly, PIT emerges at $\Delta_c/g = 0$ and $|\Delta_c|/g = 0.31$, showcasing the hierarchy $g_1^{(5)}(0) > g_1^{(4)}(0) > g_1^{(3)}(0) > g_1^{(2)}(0) > 1$. Conversely, single-PB manifests at both the two-photon resonance $\Delta_{2,-1}/g = 1.1$ and the single-photon resonance $\Delta_{1,-1}/g = 1.3$, exhibiting the sub-Poissonian statistics $g_1^{(2)}(0) < 1$. These results denote a notable progression in the exploration of non-classical photon emission, demonstrating a transducer among single-PB, PIT, 3-PB and 4-PB through the manipulation of cavity-light detuning.

Figure 5(f) further explores the interval dependence of correlation functions $g_1^{(2)}(\tau)$ and $g_4^{(2)}(\tau)$ at the four-photon resonance $\Delta_{4,\pm 2}/g = \mp 0.84$, confirming single-photon bunching ($g_1^{(2)}(0) > g_1^{(2)}(\tau)$) and four-photon bundles anti-bunching ($g_4^{(2)}(0) < g_4^{(2)}(\tau)$) with comparable lifetimes proportional to $1/\kappa$. The underlying physical mechanism for the unique non-classical photon emission relies on the high-spin degree-of-freedom atom-cavity system, which enhances optical nonlinearity and fosters interaction between

the cavity and atomic field. Interestingly, our approach facilitates the realization of multimode bundles spanning between three and four photons, thereby enabling higher-order processes to achieve higher-PB. Notably, the inherent capabilities of the high-spin degree of freedom system compensates the strong atom-cavity coupling required by the generation of strong n -PB. Our finding unveils promising avenues for studying the special non-classical quantum states, offering profound implications for advancements in quantum computing and communication [66, 67].

6. Conclusions

Building upon experimental advancements in atomic cavity QEDs, we theoretically explore the emission of n -photon bundles from a single spin-3/2 atom coupled to a single-mode optical cavity. Our investigation reveals a significant enhancement in the anharmonicity of the energy spectrum, correlated with the splitting of the n th dressed state can be significantly enhanced by adjusting the linear Zeeman shift in the spin-3/2 JCM. By appropriately driving the optical cavity and atom under the optimal linear Zeeman shift δ , we achieve the high-quality single-photon emission with $g_1^{(2)}(0) \approx 7.3 \times 10^{-4}$, as well as two-photon bundles emission with $g_1^{(2)}(0) > 1$ and $g_1^{(3)}(0) \approx 6.6 \times 10^{-4}$. A pivotal outcome of our investigation is the successful conversion from three-photon bundles to four-photon bundles emission, realized by simultaneously driving both the cavity and atom at suitable atomic-cavity detunings. These results representing a significant advancement is facilitated by the high spin degree of freedom, which compensates for the strong nonlinear interactions in our spin-3/2 JCM framework. Moreover, our study demonstrates the potential for obtaining high-quality multi-photon sources with correspondingly large steady-state photon numbers. This study provides an exceptional framework for exploring novel quantum states by harnessing spin degrees of freedom in high-spin systems, offering promising prospects for the development of non-classical quantum switches, multimode bundle splitters, and quantum information processing applications.

Acknowledgments

This work was supported by the National Natural Science Foundation of China (Grant No.12374365, Grant No. 12274473, and Grant No. 12135018) and the Fundamental Research Funds for the Central Universities (Grant No. 24qnp120).

Appendix A. Hamiltonian for spin-3/2 JCM

In this section we derive the Hamiltonian (1) based on the energy level structure and laser configuration presented in Fig. 1 in the main text. Under the rotation approximation,

the Hamiltonian of a single atom cavity coupled system is expressed as

$$\begin{aligned} \hat{\mathcal{H}}_1/\hbar = & \omega_c \hat{a}^\dagger \hat{a} + \sum_{j=1}^3 j\omega_b \hat{b}_{j+1}^\dagger \hat{b}_{j+1} + \sum_{j=1}^3 (\omega_e + j\omega'_b) \hat{e}_j^\dagger \hat{e}_j \\ & + \left[g_1 \hat{a} \sum_{j=1}^3 \hat{e}_j^\dagger \hat{b}_j + \Omega_1 \sum_{j=1}^3 \hat{e}_j^\dagger \hat{b}_{j+1} e^{-i\omega_L t} + \text{H.c.} \right], \end{aligned} \quad (\text{A.1})$$

where \hat{a}^\dagger (\hat{a}) is the creation (annihilation) operator for the cavity mode and $\hbar\omega_b$ ($\hbar\omega'_b$) represents the linear Zeeman shift within the ground (excited) state manifold. The annihilation operators for the three excited states and four ground states are respectively defined as \hat{e}_j with $j = 1, 2, 3$ and \hat{b}_j with $j = 1, 2, 3, 4$. To eliminate time dependence, we define the unitary transformation as

$$\mathcal{U} = \exp \left[-i\omega_L t \left(\hat{a}^\dagger \hat{a} + \sum_{j=1}^3 \hat{e}_j^\dagger \hat{e}_j \right) \right], \quad (\text{A.2})$$

then the Hamiltonian (A.1) can be represented as

$$\begin{aligned} \hat{\mathcal{H}}_2/\hbar = & \mathcal{U}^\dagger \hat{\mathcal{H}}_1 \mathcal{U} - i\mathcal{U}^\dagger \frac{\partial}{\partial t} \mathcal{U} \\ = & \Delta'_c \hat{a}^\dagger \hat{a} + \sum_{j=1}^3 j\omega_b \hat{b}_{j+1}^\dagger \hat{b}_{j+1} + \Delta \sum_{j=1}^3 \hat{e}_j^\dagger \hat{e}_j \\ & + \left[g_1 \hat{a} \sum_{j=1}^3 \hat{e}_j^\dagger \hat{b}_j + \Omega_1 \sum_{j=1}^3 \hat{e}_j^\dagger \hat{b}_{j+1} + \text{H.c.} \right], \end{aligned} \quad (\text{A.3})$$

where $\Delta'_c = \omega_c - \omega_L$ is the light-cavity detuning, $\Delta = \omega_e + j\omega'_b - \omega_L$ ($j = 1, 2, 3$) is the one-photon detuning of the atom. To eliminate the three excited states $|e_j\rangle$ with $j = 1, 2, 3$ the Heisenberg equations of motion for atomic operators can be written as

$$\begin{aligned} i \frac{d\hat{e}_j}{dt} &= \Delta \hat{e}_j + g_1 \hat{a} \hat{b}_j + \Omega_1 \hat{b}_{j+1} \quad (j = 1, 2, 3), \\ i \frac{d\hat{b}_1}{dt} &= g_1 \hat{a}^\dagger \hat{e}_1, \\ i \frac{d\hat{b}_2}{dt} &= \omega_b \hat{b}_2 + g_1 \hat{a}^\dagger \hat{e}_2 + \Omega_1 \hat{e}_1, \\ i \frac{d\hat{b}_3}{dt} &= 2\omega_b \hat{b}_3 + g_1 \hat{a}^\dagger \hat{e}_3 + \Omega_1 \hat{e}_2, \\ i \frac{d\hat{b}_4}{dt} &= 3\omega_b \hat{b}_4 + \Omega_1 \hat{e}_3. \end{aligned} \quad (\text{A.4})$$

Subsequently, in the dispersive regime $\Delta \gg \{g_1, \Omega_1\}$, the atomic excited states $|e_j\rangle$ with $j = 1, 2, 3$ can be adiabatically eliminated, i.e., $id\hat{e}_j/dt = 0$, which yields

$$\hat{e}_j = - \frac{g_1 \hat{a} \hat{b}_j + \Omega_1 \hat{b}_{j+1}}{\Delta}, \quad (j = 1, 2, 3). \quad (\text{A.5})$$

Substituting Eq. (A.5) into Eq. (A.4), the Heisenberg equations with respect to the ground state operators are denoted by

$$\begin{aligned}
 i\frac{d\hat{b}_1}{dt} &= -\frac{g_1^2\hat{a}^\dagger\hat{a}\hat{b}_1 + g_1\Omega_1\hat{a}^\dagger\hat{b}_2}{\Delta}, \\
 i\frac{d\hat{b}_2}{dt} &= \omega_b\hat{b}_2 - \frac{(g_1\hat{a}^\dagger\hat{a} + |\Omega_1|^2)\hat{b}_2 + g_1\Omega_1\hat{a}^\dagger\hat{b}_3 + g_1\Omega_1\hat{a}\hat{b}_1}{\Delta}, \\
 i\frac{d\hat{b}_3}{dt} &= 2\omega_b\hat{b}_3 - \frac{(g_1\hat{a}^\dagger\hat{a} + |\Omega_1|^2)\hat{b}_3 + g_1\Omega_1\hat{a}^\dagger\hat{b}_4 + g_1\Omega_1\hat{a}\hat{b}_2}{\Delta}, \\
 i\frac{d\hat{b}_4}{dt} &= 3\omega_b\hat{b}_4 - \frac{g_1\Omega_1\hat{a}\hat{b}_3 + |\Omega_1|^2\hat{b}_4}{\Delta}.
 \end{aligned} \tag{A.6}$$

Accordingly, the Hamiltonian (A.3) reduces to

$$\mathcal{H}_3/\hbar = \Delta_c\hat{a}^\dagger\hat{a} + \Delta_a\sum_{j=1}^3j\hat{b}_{j+1}^\dagger\hat{b}_{j+1} + \left[g\hat{a}^\dagger\sum_{j=1}^3\hat{b}_j^\dagger\hat{b}_{j+1} + \text{H.c.} \right], \tag{A.7}$$

where $\Delta_c = \Delta'_c - g_1^2/\Delta$ represents the effective light-cavity detuning, and $\Delta_a = \omega_b - |\Omega_1|^2/\Delta$ indicates the effective single-photon detuning. In addition, $g = -g_1\Omega_1/\Delta$ is the effective single atom-cavity coupling strength.

Furthermore, taking into account the driving terms of the cavity field and the atom field, the time-independent driven Hamiltonian under the unitary transformation (A.2) can be written as $\mathcal{H}_d = \eta(\hat{a}^\dagger + \hat{a}) + \Omega\sum_{j=1}^2\hat{b}_j^\dagger\hat{b}_{j+2} + \text{H.c.}$. As a result, the total Hamiltonian of the single atom-cavity is given by

$$\begin{aligned}
 \mathcal{H}_4/\hbar &= \Delta_c\hat{a}^\dagger\hat{a} + \Delta_a\sum_{j=1}^3j\hat{b}_{j+1}^\dagger\hat{b}_{j+1} + \eta(\hat{a}^\dagger + \hat{a}) \\
 &+ \left[g\hat{a}^\dagger\sum_{j=1}^3\hat{b}_j^\dagger\hat{b}_{j+1} + \Omega\sum_{j=1}^2\hat{b}_j^\dagger\hat{b}_{j+2} + \text{H.c.} \right],
 \end{aligned} \tag{A.8}$$

the Hamiltonian (A.8) for the spin-3/2 JCM system is the identical to Eq. (1) in the main text.

Appendix B. Eigenenergy spectrum of atom-cavity system

To deeper our understanding of the spin-3/2 JCM system, we delve into its energy spectrum. Under the scenario of weakly driven atom and cavity fields, where the total number of excitations remains constant. The Hilbert space is constrained to four Fock basis states denoted as $|n, b_1\rangle, |n-1, b_2\rangle, |n-2, b_3\rangle$ and $|n-3, b_4\rangle$, each associated with the excitation number n . The matrix M of diagonalizing the Hamiltonian (2) in the main text under the $n \geq 3$ subspace is expressed as

$$\begin{pmatrix}
 n\Delta_c & \sqrt{n}g & 0 & 0 \\
 \sqrt{n}g & (n-1)\Delta_c + \delta & \sqrt{n-1}g & 0 \\
 0 & \sqrt{n-1}g & (n-2)\Delta_c + 2\delta & \sqrt{n-2}g \\
 0 & 0 & \sqrt{n-2}g & (n-3)\Delta_c + 3\delta
 \end{pmatrix}. \tag{B.1}$$

It can be anticipated that the respective $n \geq 3$ dressed states split into four branches in the pseudospin-3/2 manifold. In order to simplify the derivation of analytical solutions, we examine the characteristic eigenenergy spectrum of the system by setting $\delta = \Delta_c$. These energy eigenvalues are represented as:

$$\begin{aligned}
 E_{n,\pm 1} &= n(\Delta_c - \Delta_{n,\pm 1}), \\
 E_{n,\pm 2} &= n(\Delta_c - \Delta_{n,\pm 2}), \\
 \Delta_{n,\pm 1} &= C_{n,\pm 1}g, \\
 \Delta_{n,\pm 2} &= C_{n,\pm 2}g, \\
 C_{n,\pm 1} &= \mp \sqrt{\frac{3n - 3 - \sqrt{5n^2 - 10n + 9}}{2n^2}}, \\
 C_{n,\pm 2} &= \mp \sqrt{\frac{3n - 3 + \sqrt{5n^2 - 10n + 9}}{2n^2}}.
 \end{aligned} \tag{B.2}$$

here $|n, \pm 2\rangle$ corresponds to the highest and lowest branches of the energy splitting of the dressed states, and $|n, \pm 1\rangle$ denote higher and lower branches. Especially, the energy splitting between the dressed states $|3, -2\rangle$ and $|3, +2\rangle$ is $2\sqrt{3 + \sqrt{6}}g$, as depicted in Fig. 1(c). Specifically, the representation of the dressed states is given by

$$\begin{aligned}
 |n, m\rangle &= \sin \theta_m \cos \varphi_m \sin \lambda_m |n, b_1\rangle \\
 &+ \sin \theta_m \sin \varphi_m \sin \lambda_m |n - 1, b_2\rangle \\
 &+ \cos \theta_m \sin \lambda_m |n - 2, b_3\rangle \\
 &+ \cos \lambda_m |n - 3, b_4\rangle \quad (m = \pm 1, \pm 2).
 \end{aligned} \tag{B.3}$$

The representation of the dressed states involves mixed angles φ_m , θ_m , and λ_m , which determine the population distribution among the different Fock states. Three mixed angles satisfy the following conditions

$$\begin{aligned}
 \tan \varphi_m &= \frac{C_{n,m}}{\sqrt{n}}, \\
 \tan \theta_m &= \frac{\sqrt{(n-1)(n + C_{n,m}^2)}}{C_{n,m}^2 - n}, \\
 \tan \lambda_m &= \frac{C_{n,m} \sqrt{(n-1)(n + C_{n,m}^2) + (C_{n,m}^2 - n)^2}}{\sqrt{(n-2)(C_{n,m}^2 - n)}}.
 \end{aligned} \tag{B.4}$$

With $m = \pm 1, \pm 2$. Figure B1 illustrates the energy spectrum of Hamiltonian (2) for various specific parameters. The resonance points in the energy spectrum correspond respectively to single-PB, two-photon bundles emission, three-photon bundles emission, and four-photon bundles emission mentioned in the main text.

Regarding two-photon excitation, the matrix of Hamiltonian (2) can be reduced to

$$\begin{pmatrix}
 n\Delta_c & \sqrt{n}g & 0 \\
 \sqrt{n}g & (n-1)\Delta_c + \delta & \sqrt{n-1}g \\
 0 & \sqrt{n-1}g & (n-2)\Delta_c + 2\delta
 \end{pmatrix}. \tag{B.5}$$

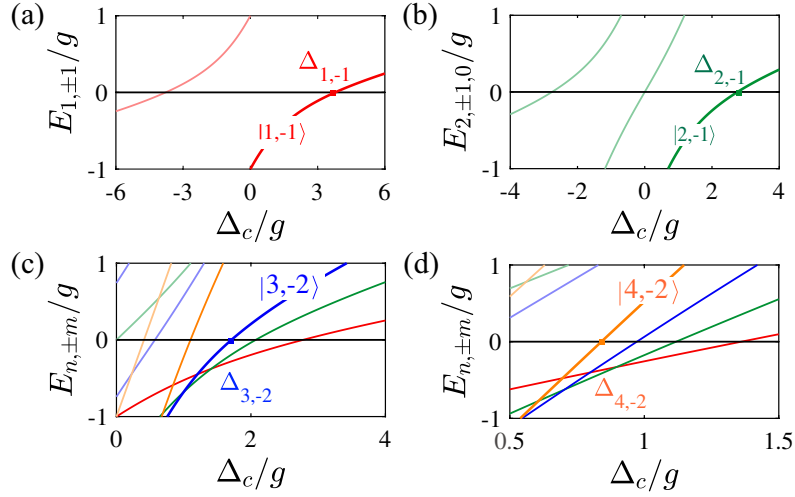


Figure B1. (Color online) The typical energy spectrum for (a) $\delta/\Delta_c = 0.04$, (b) $\delta/\Delta_c = 0.07$, (c) $\delta/\Delta_c = 0.13$, and (d) $\delta/\Delta_c = 0.54$.

Deterministically, the dressed state splits into three branches following diagonalising the Hamiltonian (B.5). The properties of the eigenenergy spectrum can be investigated more efficiently by fixing $\delta = \Delta_c$. These eigenenergy are presented by

$$\begin{aligned} E_{2,\pm 1} &= 2\Delta_c \mp \sqrt{3}g, \\ E_{2,0} &= 2\Delta_c. \end{aligned} \quad (\text{B.6})$$

As a result, the two photon resonances can be expressed as $\Delta_{2,\pm 1} = \mp\sqrt{3}g/2$ and $\Delta_{2,0} = 0$. The energy splitting between the dressed states $|2, -1\rangle$ and $|2, 0\rangle$ is given by $2\Delta_{2,-1} = \sqrt{3}g$. Conversely, the energy splitting between the dressed states $|2, -1\rangle$ and $|2, +1\rangle$ amounts to $2\sqrt{3}g$, as shown in Fig 1(c).

The corresponding eigenstates read

$$\begin{aligned} |2, +1\rangle &= -\sin\theta \cos\varphi |2, b_1\rangle + \sin\varphi |1, b_2\rangle \\ &\quad - \cos\theta \cos\varphi |0, b_3\rangle \\ |2, 0\rangle &= \cos\theta |2, b_1\rangle - \sin\theta |0, b_3\rangle \\ |2, -1\rangle &= \sin\theta \sin\varphi |2, b_1\rangle + \cos\varphi |1, b_2\rangle \\ &\quad + \cos\theta \sin\varphi |0, b_3\rangle \end{aligned} \quad (\text{B.7})$$

where two mixed angles need to satisfy

$$\begin{aligned} \tan\theta &= \sqrt{2}, \\ \tan\varphi &= 1. \end{aligned} \quad (\text{B.8})$$

Concerning the process of single-photon excitation, the matrix of Hamiltonian (2) is reduced to

$$\begin{pmatrix} n\Delta_c & \sqrt{n}g \\ \sqrt{n}g & (n-1)\Delta_c + \delta \end{pmatrix}. \quad (\text{B.9})$$

Upon diagonalizing the Hamiltonian (B.9), the dressed states are found to bifurcate into two branches, with corresponding eigenenergies given by $E_{1,\pm 1} = (\Delta_c + \delta)/2 \pm \sqrt{g^2 + (\delta - \Delta_c)^2}/4$. By fixing $\delta = \Delta_c$ in Fig. 1 (c), the eigenenergies simplify to $E_{1,\pm 1} = \Delta_c \mp g$. Consequently, the single photon resonance can be characterized by $\Delta_{1,\pm 1} = \mp g$. The energy splitting between the dressed states $|1, -1\rangle$ and $|1, +1\rangle$ is $2g$.

Specifically, the eigenstates can be written as

$$\begin{aligned} |1, +1\rangle &= \sin \theta |1, b_1\rangle - \cos \theta |0, b_2\rangle, \\ |1, -1\rangle &= \cos \theta |1, b_1\rangle + \sin \theta |0, b_2\rangle, \end{aligned} \tag{B.10}$$

where the mixed angle meets the following conditions

$$\tan \theta = \sqrt{\frac{\varepsilon - (\delta - \Delta_c)}{\varepsilon + (\delta - \Delta_c)}}, \tag{B.11}$$

with $\varepsilon = \sqrt{(\delta - \Delta_c)^2 + 4g^2}$.

In summary, the anharmonicity energy spectrum can be sketched as shown in Fig. 1(c).

Data availability statement

All data that support the findings of this study are included within the article (and any supplementary files).

References

- [1] L.-M. Duan, M. D. Lukin, J. I. Cirac, and P. Zoller. Long-distance quantum communication with atomic ensembles and linear optics. *Nature*, 414:413–418, Nov 2001.
- [2] C. H. Bennett and D. P. DiVincenzo. Quantum information and computation. *Nature*, 404:247–255, Mar 2000.
- [3] P. Kok, W. J. Munro, K. Nemoto, T. C. Ralph, J. P. Dowling, and G. J. Milburn. Linear optical quantum computing with photonic qubits. *Rev. Mod. Phys.*, 79:135–174, Jan 2007.
- [4] V. Giovannetti, S. Lloyd, and L. Maccone. Quantum metrology. *Phys. Rev. Lett.*, 96:010401, Jan 2006.
- [5] P. Luca, A. Smerzi, M. K. Oberthaler, R. Schmied, and P. Treutlein. Quantum metrology with nonclassical states of atomic ensembles. *Rev. Mod. Phys.*, 90:035005, Sep 2018.
- [6] D. Braun, G. Adesso, F. Benatti, R. Floreanini, U. Marzolino, M. W. Mitchell, and S. Pirandola. Quantum-enhanced measurements without entanglement. *Rev. Mod. Phys.*, 90:035006, Sep 2018.
- [7] M. Lei, R. Fukumori, J. Rochman, B.-H. Zhu, M. Endres, J. Choi, and A. Faraon. Many-body cavity quantum electrodynamics with driven inhomogeneous emitters. *Nature*, 617:271–276, May 2023.
- [8] C. J. Villas-Boas and D. Z. Rossatto. Multiphoton jaynes-cummings model: Arbitrary rotations in fock space and quantum filters. *Phys. Rev. Lett.*, 122:123604, Mar 2019.
- [9] W. Leonski and A. Kowalewska-Kudlaszyk. Quantum scissors finite-dimensional states engineering. 56:131–185, 2011.
- [10] W. Leoński and R. Tanaś. Possibility of producing the one-photon state in a kicked cavity with a nonlinear kerr medium. *Phys. Rev. A*, 49:R20–R23, Jan 1994.

- [11] A. Ridolfo, M. Leib, S. Savasta, and M. J. Hartmann. Photon blockade in the ultrastrong coupling regime. *Phys. Rev. Lett.*, 109:193602, Nov 2012.
- [12] T. C. H. Liew and V. Savona. Single photons from coupled quantum modes. *Phys. Rev. Lett.*, 104:183601, May 2010.
- [13] M. Bamba, A. Imamoğlu, I. Carusotto, and C. Ciuti. Origin of strong photon antibunching in weakly nonlinear photonic molecules. *Phys. Rev. A*, 83:021802, Feb 2011.
- [14] A. Majumdar, M. Bajcsy, A. Rundquist, and J. Vučković. Loss-enabled sub-poissonian light generation in a bimodal nanocavity. *Phys. Rev. Lett.*, 108:183601, May 2012.
- [15] K. M. Birnbaum, A. Boca, R. Miller, A. D. Boozer, T. E. Northup, and H. J. Kimble. Photon blockade in an optical cavity with one trapped atom. *Nature*, 436:87–90, Jul 2005.
- [16] J. M. Fink, M. Göppl, M. Baur, R. Bianchetti, P. J. Leek, A. Blais, and A. Wallraff. Climbing the jaynes-cummings ladder and observing its \sqrt{n} nonlinearity in a cavity qed system. *Nature*, 454:315–318, Jul 2008.
- [17] J. Tang, Y.-G. Deng, and C.-H. Lee. Tunable photon blockade with a single atom in a cavity under electromagnetically induced transparency. *Photon. Res.*, 9(7):1226–1233, Jul 2021.
- [18] J. Tang, W.-D Geng, and X.-L. Xu. Quantum interference induced photon blockade in a coupled single quantum dot-cavity system. *Sci. Rep.*, 5:9252, Mar 2015.
- [19] Y.-L. Liu, G.-Z. Wang, Y.-X. Liu, and F. Nori. Mode coupling and photon antibunching in a bimodal cavity containing a dipole quantum emitter. *Phys. Rev. A*, 93:013856, Jan 2016.
- [20] A. J. Hoffman, S. J. Srinivasan, S. Schmidt, L. Spietz, J. Aumentado, H. E. Türeci, and A. A. Houck. Dispersive photon blockade in a superconducting circuit. *Phys. Rev. Lett.*, 107:053602, Jul 2011.
- [21] Y.-X. Liu, X.-W. Xu, A. Miranowicz, and F. Nori. From blockade to transparency: Controllable photon transmission through a circuit-qed system. *Phys. Rev. A*, 89:043818, Apr 2014.
- [22] S. Ferretti, L. C. Andreani, H. E. Türeci, and D. Gerace. Photon correlations in a two-site nonlinear cavity system under coherent drive and dissipation. *Phys. Rev. A*, 82:013841, Jul 2010.
- [23] S. Ghosh and T. C. H. Liew. Dynamical blockade in a single-mode bosonic system. *Phys. Rev. Lett.*, 123:013602, Jul 2019.
- [24] H. Z. Shen, Y.-H. Zhou, and X.-X. Yi. Tunable photon blockade in coupled semiconductor cavities. *Phys. Rev. A*, 91:063808, Jun 2015.
- [25] H. Flayac and V. Savona. Unconventional photon blockade. *Phys. Rev. A*, 96:053810, Nov 2017.
- [26] P. Rabl. Photon blockade effect in optomechanical systems. *Phys. Rev. Lett.*, 107:063601, Aug 2011.
- [27] A. Nunnenkamp, K. Børkje, and S. M. Girvin. Single-photon optomechanics. *Phys. Rev. Lett.*, 107:063602, Aug 2011.
- [28] F. Zou, L.-B. Fan, J.-F. Huang, and J.-Q. Liao. Enhancement of few-photon optomechanical effects with cross-kerr nonlinearity. *Phys. Rev. A*, 99:043837, Apr 2019.
- [29] B.-J. Li, R. Huang, X.-W. Xu, A. Miranowicz, and H. Jing. Nonreciprocal unconventional photon blockade in a spinning optomechanical system. *Photon. Res.*, 7(6):630–641, Jun 2019.
- [30] A. Miranowicz, M. Paprzycka, Y.-X. Liu, J. Bajer, and F. Nori. Two-photon and three-photon blockades in driven nonlinear systems. *Phys. Rev. A*, 87:023809, Feb 2013.
- [31] C. Hamsen, K. N. Tolazzi, T. Wilk, and G. Rempe. Two-photon blockade in an atom-driven cavity qed system. *Phys. Rev. Lett.*, 118:133604, Mar 2017.
- [32] W.-W. Deng, G.-X. Li, and H. Qin. Enhancement of the two-photon blockade in a strong-coupling qubit-cavity system. *Phys. Rev. A*, 91:043831, Apr 2015.
- [33] S. S. Shamailov, A. S. Parkins, M. J. Collett, and H. J. Carmichael. Multi-photon blockade and dressing of the dressed states. *Opt. Commun.*, 283(5):766–772, 2010.
- [34] Q. Bin, X.-Y. Lü, S.-W. Bin, and Y. Wu. Two-photon blockade in a cascaded cavity-quantum-electrodynamics system. *Phys. Rev. A*, 98:043858, Oct 2018.
- [35] C. J. Zhu, Y. P. Yang, and G. S. Agarwal. Collective multiphoton blockade in cavity quantum

- electrodynamics. *Phys. Rev. A*, 95:063842, Jun 2017.
- [36] J. Z. Lin, K. Hou, C. J. Zhu, and Y. P. Yang. Manipulation and improvement of multiphoton blockade in a cavity-qed system with two cascade three-level atoms. *Phys. Rev. A*, 99:053850, May 2019.
- [37] G. H. Hovsepyan, A. R. Shahinyan, and G. Y. Kryuchkyan. Multiphoton blockades in pulsed regimes beyond stationary limits. *Phys. Rev. A*, 90:013839, Jul 2014.
- [38] R. Huang, A. Miranowicz, J.-Q. Liao, F. Nori, and H. Jing. Nonreciprocal photon blockade. *Phys. Rev. Lett.*, 121:153601, Oct 2018.
- [39] I. Afek, O. Ambar, and Y. Silberberg. High-noon states by mixing quantum and classical light. *Science*, 328(5980):879–881, 2010.
- [40] M. D’Angelo, M. V. Chekhova, and Y. Shih. Two-photon diffraction and quantum lithography. *Phys. Rev. Lett.*, 87:013602, Jun 2001.
- [41] H. J. Kimble. The quantum internet. *Nature*, 453:1023–1030, Jun 2008.
- [42] N. G. Horton, K. Wang, D. Kobat, C. G. Clark, F. W. Wise, C. B. Schaffer, and C. Xu. In vivo three-photon microscopy of subcortical structures within an intact mouse brain. *Nat. Photon.*, 7:205–209, Jan 2013.
- [43] Y.-G. Deng, T. Shi, and S. Yi. Motional n-phonon bundle states of a trapped atom with clock transitions. *Photon. Res.*, 9(7):1289–1299, Jul 2021.
- [44] J. Zakrzewski, M. Lewenstein, and T. W. Mossberg. Theory of dressed-state lasers. i. effective hamiltonians and stability properties. *Phys. Rev. A*, 44:7717–7731, Dec 1991.
- [45] C. S. Muñoz, E. Del Valle, A. G. Tudela, K. Müller, S. Lichtmannecker, M. Kaniber, C. Tejedor, J. J. Finley, and F. P. Laussy. Emitters of n-photon bundles. *Nat. photon.*, 8:550–555, Jun 2014.
- [46] C. S. Muñoz, F. P. Laussy, E. del Valle, C. Tejedor, and A. González-Tudela. Filtering multiphoton emission from state-of-the-art cavity quantum electrodynamics. *Optica*, 5(1):14–26, Jan 2018.
- [47] J. C. López Carreño, E. del Valle, and F. P. Laussy. Photon correlations from the mollow triplet. *Laser Photonics Rev.*, 11(5):1700090, 2017.
- [48] Y. Chang, A. González-Tudela, C. Sánchez Muñoz, C. Navarrete-Benlloch, and T. Shi. Deterministic down-converter and continuous photon-pair source within the bad-cavity limit. *Phys. Rev. Lett.*, 117:203602, Nov 2016.
- [49] K. Koshino, T. Shitara, Z. Ao, and K. Semba. Deterministic three-photon down-conversion by a passive ultrastrong cavity-qed system. *Phys. Rev. Res.*, 4:013013, Jan 2022.
- [50] C. Zhang, Y.-F. Huang, B.-H. Liu, C.-F. Li, and G.-C. Guo. Spontaneous parametric down-conversion sources for multiphoton experiments. *Adv. Quantum Technol.*, 4(5):2000132, 2021.
- [51] Q. Bin, X.-Y. Lü, F. P. Laussy, F. Nori, and Y. Wu. N-phonon bundle emission via the stokes process. *Phys. Rev. Lett.*, 124:053601, Feb 2020.
- [52] Q. Bin, Y. Wu, and X.-Y. Lü. Parity-symmetry-protected multiphoton bundle emission. *Phys. Rev. Lett.*, 127:073602, Aug 2021.
- [53] J. Tang and Y.-G. Deng. Strong single-photon to two-photon bundles emission in spin-1 Jaynes-Cummings model. *APL Photonics*, 8(7):076103, 07 2023.
- [54] M. Zhang, L.-T. Feng, Z.-Y. Zhou, Y. Chen, H. Wu, M. Li, S.-M. Gao, G.-P. Guo, G.-C. Guo, D.-X. Dai, and X.-F. Ren. Generation of multiphoton quantum states on silicon. *Light: Sci. Appl.*, 8:41, May 2019.
- [55] P. Thomas, L. Ruscio, O. Morin, and G. Rempe. Efficient generation of entangled multiphoton graph states from a single atom. *Nature*, 608:677–681, Aug 2022.
- [56] L. Li, Z.-X. Liu, X.-F. Ren, S.-M. Wang, V.-C. Su, M.-K. Chen, C.-H. Chu, H. Y. Kuo, B.-H. Liu, W.-B. Zang, G.-C. Guo, L.-J. Zhang, Z.-L. Wang, S.-N. Zhu, and D. P. Tsai. Metalens-array based high-dimensional and multiphoton quantum source. *Science*, 368(6498):1487–1490, 2020.
- [57] N. Gisin, G. Ribordy, W. Tittel, and H. Zbinden. Quantum cryptography. *Rev. Mod. Phys.*, 74:145–195, Mar 2002.
- [58] S. M. Tan. A computational toolbox for quantum and atomic optics. *J. Opt. B: Quantum and*

- Semiclassical Opt.*, 1(4):424, aug 1999.
- [59] R. J. Glauber. The quantum theory of optical coherence. *Phys. Rev.*, 130:2529–2539, Jun 1963.
 - [60] H. J. Carmichael. *statistical methods in quantum optics 1: master equations and fokker – planck equations.* (Springer Science & Business Media 2013), Jun.
 - [61] A. Faraon, I. Fushman, D. Englund, N. Stoltz, P. Petroff, and J. Vučković. Coherent generation of non-classical light on a chip via photon-induced tunnelling and blockade. *Nat. Phys.*, 4:859–863, Nov 2008.
 - [62] Marco Mancini, Guido Pagano, Giacomo Cappellini, Lorenzo Livi, Marie Rider, Jacopo Catani, Carlo Sias, Peter Zoller, Massimo Inguscio, Marcello Dalmonte, et al. Observation of chiral edge states with neutral fermions in synthetic hall ribbons. *Science*, 349(6255):1510–1513, 2015.
 - [63] T. A. Zheng, Y. A. Yang, S.-Z. Wang, J. T. Singh, Z.-X. Xiong, T. Xia, and Z.-T. Lu. Measurement of the electric dipole moment of ^{171}Yb atoms in an optical dipole trap. *Phys. Rev. Lett.*, 129:083001, Aug 2022.
 - [64] M. A. Norcia, M. N. Winchester, J. R. K. Cline, and J. K. Thompson. Superradiance on the millihertz linewidth strontium clock transition. *Sci. Adv.*, 2(10):e1601231, 2016.
 - [65] Yuangang Deng, Tao Shi, and Su Yi. Motional n-phonon bundle states of a trapped atom with clock transitions. *Photonics Research*, 9(7):1289–1299, 2021.
 - [66] P. Thomas, L. Ruscio, O. Morin, and G. Rempe. Efficient generation of entangled multiphoton graph states from a single atom. *Nature*, 608:677–681, Aug 2022.
 - [67] C.-W. Yang, Y. Yu, J. Li, B. Jing, X.-H. Bao, and J.-W. Pan. Sequential generation of multiphoton entanglement with a rydberg superatom. *Nat. Photon.*, 16:658–661, Sep 2022.